A novel procedure for damage evaluation of fillet-welded joints

**Submitted to International Journal of Fatigue**, January 2020
VSI: Fatigue of Welded Joints – Current State-of-the-Art
**Version R1, March 2020**

# A NOVEL PROCEDURE FOR DAMAGE EVALUATION OF FILLET-WELDED JOINTS

Sabrina Vantadori[1], Ignacio Iturrioz[2], Andrea Carpinteri[1],
Fabrizio Greco[3], Camilla Ronchei[3]

[1]Department of Engineering & Architecture, University of Parma,
Parco Area delle Scienze 181/A, 43124 Parma, Italy

[2]Mechanical Post- Graduate Program, Federal University of Rio Grande do Sul,
Sarmento Leite 425, CEP 90050-170, Porto Alegre, Brazil

[3]Department of Civil Engineering, University of Calabria,
via Pietro Bucci, 87036 Arcavacata di Rende (CS), Italy

**ABSTRACT**

In the present paper, a novel procedure for fatigue resistance assessment of fillet-welded joints under complex random loading is proposed. It consists of two consecutive steps: (1) computation of the stress tensor at the verification point; (2) evaluation of damage and, consequently, fatigue life. The procedure exploits the multiaxial critical plane-based criterion by Carpinteri et al. for random loading. A case study, represented by a mechanical component of an arm sprayer used in agriculture, is examined in order to assess such a procedure. A comparison between experimental and numerical results in terms of crack nucleation location is performed.

**KEYWORDS:** critical plane, hot spot, multiaxial, random loading

**NOMENCLATURE**

| | |
|---|---|
| $\mathbf{C}$ | vector lying on the critical plane |
| $C_a^*$ | amplitude of $\mathbf{C}^*$ in a given reversal |
| $\mathbf{C}_i$ | vector series of $\mathbf{C}$ |
| $\mathbf{C}_i^*$ | reduced vector series of $\mathbf{C}$ |
| $C_u$ , $C_v$ | components of $\mathbf{C}$ along the directions u and v, respectively |
| $C_{u,i}$ , $C_{v,i}$ | scalar series of the modulus of the $\mathbf{C}$ components |
| $D(T_0)$ | damage accumulated during the observation period $T_0$ |
| $D_{cr}$ | critical damage |
| $F_b$ , $F_c$ | forces applied to the H component FE model |
| $F_b^m$ , $F_c^m$ | forces applied to the H component FE model in order to simulate the $m$-th maneuver |
| $H$ | Hot spot |
| $m$ | maneuver number (see Table 1) |
| $n$ | number of elements of both $\mathbf{N}$- and $\mathbf{C}$-series |
| $\mathbf{N}$ | vector perpendicular to the critical plane |
| $N_i$ | scalar series of the $\mathbf{N}$ modulus |
| $N_i^*$ | reduced scalar series of $\mathbf{N}$ |
| $N_{\max}^*$ | maximum value of $\mathbf{N}^*$ in a given reversal |
| $Or\alpha$ | polar frame |
| $\mathbf{S_w}$ | stress vector at the verification point |
| $T$ | plate thickness or thickness of both the chord and the brace for the case study examined |
| $T_f$ | fatigue life |
| $T_0$ | observation period |
| $\overline{T}$ | observation time interval for the case study examined |
| uvw | local frame attached to the critical plane |
| XYZ | fixed frame |

| | |
|---|---|
| $\mathbf{w}$ | normal to the critical plane |
| $W$ | weight function |
| W1,W2,W3 | control points |
| $\hat{1},\hat{2},\hat{3}$ | averaged principal stress directions |

| | |
|---|---|
| $\alpha$ | orientation of a generic extrapolation path |
| $\delta$ | angle between $\hat{1}$ and $\mathbf{w}$ |
| $\varepsilon_{1,b}^{exp,m}$ | experimental maximum principal strain time-history at point W3 |
| $\varepsilon_{1,b}^{num}$ | numerical maximum principal strain at point W3 computed for $F_b = 1N$ |
| $\varepsilon_{1,c}^{exp,m}$ | experimental maximum principal strain time-history at point W1, or equivalently, at point W2 |
| $\varepsilon_{1,c}^{num}$ | numerical maximum principal strain at point W1 computed for $F_c = 1N$ |
| $\phi,\theta,\psi$ | principal Euler angles |
| $\hat{\phi},\hat{\theta},\hat{\psi}$ | averaged principal Euler angles |
| $\sigma_{af,-1}$ | fatigue strength under fully reversed normal stress (evaluated at $N_0$ loading cycles) |
| $\sigma_{eq,a}^{(j)}$ | amplitude of the equivalent stress related to the $j$-th reversal |
| $\sigma_{x,hs}$ | $\sigma_x$ at the hot spot |
| $\sigma_{y,hs}$ | $\sigma_y$ at the hot spot |
| $\tau_{xy,hs}$ | $\tau_{xy}$ at the hot spot |
| $\sigma_{1,\max}$ | maximum value of the maximum principal stress $\sigma_1$ |
| $\tau_{af,-1}$ | fatigue strength under fully reversed shear stress (evaluated at $N_0^*$ loading cycles) |

## 1. INTRODUCTION

Fillet-welded joints, in the form of "T" joint, lap joint and corner joint, represent the most common connections in welded structures. Fillet-welded joints combine different advantages such as lightness of structures, high flexibility in geometrical design, and cost saving due to both reduced fabrication time and less manufacture effort. Despite of this, fillet-welded joints can also represent the weakest part of welded structures with respect to failure, since their breakdown is generally due to fatigue-induced failure, approximatively in 90% of cases **[1]**. Data in the literature cover different fatigue failure modes **[1,2]**, the most common ones under service conditions being produced by crack initiation and propagation (a) at weld toes and running into the parent material, (b) at weld root and running into the weld throat, and (c) at discontinuities inside the weld and running into welding/parent material.

For welded structures under simple cyclic loading (i.e. tension-compression or cyclic bending or others), international fatigue design rules employing procedures based on fatigue strength S-N curves are now widely available **[3-5]**, although local stress approach and crack initiation-based fatigue life approach represent alternatives for fatigue life evaluation related to welded structures **[6-8]**.

More precisely, according to the "Recommendations for fatigue design of welded joints and components" **[5]**, the above procedures based on fatigue strength S-N curves differ from each other for the

stress range (computed or measured) employed to perform such an assessment. Three approaches have been proposed in Ref.**[5]**: (i) nominal stress approach, (ii) structural hot spot stress approach, (iii) effective notch stress approach.

As a matter of fact, the stress range may include or exclude the local stress raising effect coming from (1) discontinuity due to a structural detail of welded joint and (2) weld toe transition. More precisely:

(i) Nominal stress approach: the stress range is computed or measured by exluding the local stress raising effect due to both discontinuity and transition;

(ii) Structural hot spot stress approach: the stress range is computed or measured by including the local stress raising effect due to the above discontinuity, but excluding that due to the above transition;

(iii) Effective notch stress approach: the stress range is computed or measured by including the local stress raising effect due to both discontinuity and transition.

**Figure 1** shows the stress computed at a given time instant, according to the above three approaches.

**Figure 1.**

Note that, when large cutouts are present in the vicinity of the welded joint, their local stress raising effects have to be included in the computed or measured stress range.

For welded structures under complex cyclic loading (i.e. multiaxial), the most common design approaches are based on the maximum principal stress range or equivalent stress range, then referred to fatigue strength S-N curves, the same ones used for welded structures under simple cyclic loading **[9]**. However, there are extensive experimental data showing that the above approaches can overestimate the fatigue life of welded structures even by an order of magnitude under non-proportional loading **[9]**. As a matter of fact, fatigue life under non-proportional loading decreases with respect to that under proportional loading, and that is due to: (i) additional hardening effect, or (ii) initiation of more micro-cracks produced by the activation of more slip systems in grains, as a consequence of the change of principal stress/strain directions. Therefore, when a given approach does not take into account the above phenomena, fatigue life may be overestimated. This drawback has prompted the research work towards the development of alternative methods to be used in fatigue assessment of welded structures under complex cyclic loading **[10-30]**.

In such a context, a novel procedure for fatigue resistance assessment of fillet-welded joints under complex random loading is herein proposed. Such a procedure consists of two consecutive steps: (1) computation of the stress tensor at the verification point (hot spot), according to the extrapolation equation derived through the structural hot spot stress approach **[5]**; (2) evaluation of damage (at the same verification point) and, consequently fatigue life, by applying the multiaxial critical plane-based criterion by Carpinteri

et al. for random loading **[31-34]**. To the best knowledge of the authors, a similar procedure has not been proposed in the literature yet.

In order to verify the above novel procedure, data available in the literature are employed **[35-39]**. More precisely, a fillet-welded structure represented by the H component of an arm sprayer used in agriculture is analysed (**Figure 2**).

**Figure 2.**

As a matter of fact, the H component is constituted from welded tubular elements, fillet-welded as T-joints. Each joint consists of two tubular elements: one with a rectangular cross-section, named chord, and the other one with a circular cross-section, named brace. Under the arm sprayer service condition, the whole H component is subjected to high-cycle random fatigue loading and, consequently, each of its T-joints experiences a multiaxial random stress field.

The novel procedure is applied to that T-joint of the H component where fatigue failure is experimentally observed (**Figure 3**), in order to evaluate the region on the weld toe where cracks are expected to nucleate.

**Figure 3.**

The paper is organised as follows. Section 2 is dedicated to the description of the novel procedure. In Section 3, the case study is presented by giving details on the geometry and the stress field

that characterise the fillet T-joint examined, and on the damage evaluation. The results obtained are discussed in Section 4, and conclusions are summarised in Section 5.

## 2. THE NOVEL PROCEDURE

Firstly, the proposed procedure requires to compute the stress state at the verification point and then the accumulated damage at the same point.

### 2.1 Computation of the stress tensor components at the verification point

Let us consider the point $H$ in **Figure 4**, assumed as the hot spot, and the extrapolation path perpendicular to the weld **[5]**.

**Figure 4.**

The stress state at a generic point along the above path is biaxial, that is, the stress tensor components different from zero are $\sigma_x, \sigma_y$, and $\tau_{xy}$. In order to compute the values of such components at the hot spot, the extrapolation equation derived through the structural hot spot stress approach for type "a" hot spot and coarse mesh **[5]** is employed, that is:

$$\sigma_{x,hs} = 1.5\sigma_{x(0.5T)} - 0.5\sigma_{x(1.5T)} \quad \textbf{(1)}$$

$$\sigma_{y,hs} = 1.5\sigma_{y(0.5T)} - 0.5\sigma_{y(1.5T)} \quad \textbf{(2)}$$

$$\tau_{xy,hs} = 1.5\tau_{xy(0.5T)} - 0.5\tau_{xy(1.5T)} \quad \textbf{(3)}$$

where the stresses with the subscripts $0.5T$ and $1.5T$ are those at two reference points which are $0.5T$ and $1.5T$ away from $H$ along the extrapolation path, respectively, being $T$ the plate thickness.

### 2.2 Damage and fatigue life computation

In order to compute damage and consequently the fatigue life, the multiaxial critical plane-based criterion by Carpinteri et al. for random loading, formulated in time-domain, is employed **[31-34]**. The criterion is here applied in the form that implements the recent modifications proposed in Ref.**[34]**.

Let us consider a verification point and a fixed frame XYZ with its origin in such a point. According to the above criterion, the principal Euler angles $\phi,\theta,\psi$ at the verification point are averaged as follows:

$$\hat{\phi} = \frac{1}{W}\int_0^{T_0} \phi(t) W(t)\, dt \qquad (4)$$

$$\hat{\theta} = \frac{1}{W}\int_0^{T_0} \theta(t) W(t)\, dt \qquad (5)$$

$$\hat{\psi} = \frac{1}{W}\int_0^{T_0} \psi(t) W(t)\, dt \qquad (6)$$

where

$$W = \int_0^{T_0} W(t)\, dt \qquad (7)$$

and the weight function $W(t)$ is given by:

$$H[x] = 1 \quad \text{for } x \geq 0 \qquad (8)$$

$$W(t) = H\left[\sigma_1(t) - \sigma_{1,\max}\right] \qquad H[x] = 0 \ \text{ for } \ x < 0$$

being $\sigma_{1,\max}$ the maximum value of the maximum principal stress $\sigma_1(t)$ during the observation period $T_0$. By using the above angles $\hat{\phi}, \hat{\theta}, \hat{\psi}$, the averaged principal stress directions $\hat{1}, \hat{2}, \hat{3}$ are identified.

The normal $\mathbf{w}$ to the critical plane is assumed to belong to the principal plane $\hat{1}\hat{3}$, and its direction is determined by rotating $\hat{1}$-axis towards $\hat{3}$-axis of an angle expressed by (in degrees):

$$\delta = \frac{3}{2}\left[1 - \left(\frac{\tau_{af,-1}}{\sigma_{af,-1}}\right)^2\right] 45° \tag{9}$$

where $\tau_{af,-1}$ is the fatigue strength under fully reversed shear stress (evaluated at $N_0^*$ loading cycles), whereas $\sigma_{af,-1}$ is the fatigue strength under fully reversed normal stress (evaluated at $N_0$ loading cycles).

Once the critical plane passing through the verification point is identified, a local frame $\mathbf{uvw}$ is adopted, where the $\mathbf{u}$-direction is represented by the intersection line between the critical plane and the $\mathbf{wZ}$ plane, and $\mathbf{v}$ forms an orthogonal frame with $\mathbf{u}$ and $\mathbf{w}$. The stress vector $\mathbf{S_w}$ at the verification point may be decomposed as follows:

$$\mathbf{S_w} = \mathbf{N} + \mathbf{C} \tag{10}$$

where $\mathbf{N}$ is perpendicular to the critical plane, whereas $\mathbf{C}$ lies on such a plane and may be decomposed in two components, $C_u$ and $C_v$, along the directions $\mathbf{u}$ and $\mathbf{v}$, respectively.

Let us consider the scalar series $N_i$ of the modulus of $\mathbf{N}$, and the vector series $\mathbf{C}_i$ of the vector $\mathbf{C}$, each series being composed by $n$ elements (i.e. $0 \le i \le n$). Note that $\mathbf{C}$-series can be also equivalently represented by the two scalar series of its components, named $C_{u,i}$ and $C_{v,i}$.

A reduction procedure is performed on $\mathbf{N}$-series in order to preserve only peaks and valleys of this series, and a new one, named $\mathbf{N}^*$-series, is obtained. As an example, let us consider three terms of the $\mathbf{N}$-series, that is, $N_i, N_{i+1}$ and $N_{i+2}$, where $N_i$ is a peak and $N_{i+2}$ is a valley, i.e. $N_i > N_{i+2}$. The indexes of the latter terms are registered in a vector of two components, $\mathbf{K} \equiv (k_1, k_2)$: in this case, we have $\mathbf{K} \equiv (i, i+2)$. The reduction procedure operates as follows:

$$N_i^* = N_{k_1} \qquad N_{i+1}^* = \frac{N_{k_1} + N_{k_2}}{2} \qquad N_{i+2}^* = N_{k2} \tag{11}$$

In such a way, the number of terms for the $\mathbf{N}$- and $\mathbf{N}^*$-series is the same and equal to $n$.

A reduction procedure is also performed on the $\mathbf{C}$-series in order to preserve only the vectors that maximise the amplitude of $\mathbf{C}$ between a peak and a valley of the $\mathbf{N}$-series. In more detail, if we consider the above case, i.e. $\mathbf{K} \equiv (i, i+2)$, the following amplitudes are computed according to the definition by Papadopoulos [**40**]:

$$C_{a(i,i+1)} = \sqrt{\left[C_{u,i+1} - \frac{1}{2}\left(C_{u,i} + C_{u,i+1}\right)\right]^2 + \left[C_{v,i+1} - \frac{1}{2}\left(C_{v,i} + C_{v,i+1}\right)\right]^2} \tag{12}$$

$$C_{a(i,i+2)} = \sqrt{\left[C_{u,i+2} - \frac{1}{2}\left(C_{u,i} + C_{u,i+2}\right)\right]^2 + \left[C_{v,i+2} - \frac{1}{2}\left(C_{v,i} + C_{v,i+2}\right)\right]^2} \qquad \textbf{(13)}$$

Then, if $C_{a(i,i+1)} \le C_{a(i,i+2)}$, we get:

$$\mathbf{C}_i^* = \mathbf{C}_{k_1} \qquad \mathbf{C}_{i+1}^* = \frac{\mathbf{C}_{k_1} + \mathbf{C}_{k_2}}{2} \qquad \mathbf{C}_{i+2}^* = \mathbf{C}_{k2} \qquad \textbf{(14)}$$

whereas, if $C_{a(i,i+1)} > C_{a(i,i+2)}$, we get:

$$\mathbf{C}_i^* = \mathbf{C}_{k_1} \qquad \mathbf{C}_{i+1}^* = \frac{\mathbf{C}_{k_1} + \mathbf{C}_{i+1}}{2} \qquad \mathbf{C}_{i+2}^* = \mathbf{C}_{i+1} \qquad \textbf{(15)}$$

In such a way, the number of terms for $\mathbf{C}$- and $\mathbf{C}^*$-series is the same and equal to $n$. The above two conditions on the $\mathbf{C}$ amplitudes are graphically shown in **Figure 5**. Furthermore, a numerical example of the above reduction procedure is reported in Ref.**[34]**.

**Figure 5.**

The rainflow counting method is applied to the $\mathbf{N}^*$-series. For each counted reversal, the maximum value of $\mathbf{N}^*$ and the amplitude of $\mathbf{C}^*$ computed as proposed in Ref.**[40]** are registered in order to determine the following equivalent stress amplitude:

$$\sigma_{eq,a} = \sqrt{\left(N_{\max}^*\right)^2 + \left(\frac{\sigma_{af,-1}}{\tau_{af,-1}}\right)^2 \left(C_a^*\right)^2} \qquad \textbf{(16)}$$

The damage accumulated during the observation period $T_0$ is computed by applying the Palmgren-Miner rule:

$$D(T_0) = \sum_{j=1}^{J} \frac{1}{2 \cdot N_0 \left( \frac{\sigma_{af,-1}}{\sigma_{eq,a}^{(j)}} \right)^{-\frac{1}{k}}} \quad \textbf{(17)}$$

where $\sigma_{eq,a}^{(j)}$ is the amplitude of the equivalent stress related to the $j$-th reversal (computed according to Eq.(16)), and $J$ is the total number of counted reversals. Consequently, the fatigue life is given by:

$$T_f = D_{cr} \frac{T_0}{D(T_0)} \quad \textbf{(18)}$$

where $D_{cr}$ is the critical damage.

## 3. APPLICATION OF THE NOVEL PROCEDURE: A CASE STUDY

The case study here examined is represented by the top fillet-welded T-joint on the right-hand side of the H component shown in **Figure 6**, which is the weakest T-joint with regard to fatigue failure under service condition **[35]**, as has been experimentally observed. The welding has been performed by means of a metal inert gas process. The leg length of welding is equal to 5mm.

**Figure 6.**

Such a component is a part of an arm sprayer, which is an agricultural machine used to pulverize herbicides and fungicides in order to preserve crops against harmful insects and herbs. Under

sprayer service condition, the H component and consequently its T-joints are subjected to high-cycle fatigue random loading.

This component has already been analysed by the present authors in Refs **[36-39]** considering not the actual random loading acting on the H component, but an equivalent loading constituted by forces with a constant amplitude.

### 3.1 Multiaxial random stress field

The random stress field in the T-joint has been determined by employing both experimental measurements and finite element analysis **[35]**. Since a severe crack pattern in the H component is usually highlighted after 2000h of sprayer operation (see **Figure 3**), such a time interval is assumed to be the observation time interval $\overline{T}$.

A typical service condition of the sprayer being examined, represented by the application of herbicides in crops of a Brazilian city (Jaboticabal, São Paulo), consists of 12 maneuvers repeated many times during $\overline{T}$. The duration of each of such 12 maneuvers is listed in **Table 1**, together with how many times each maneuver is repeated during $\overline{T}$.

Note that each maneuver was performed twice a day: one when the tractor fuel tank was full, and the other one when the fuel tank was empty. More precisely (**Table 1**):

(a) Shifting the tractor, dragging the agricultural sprayer from the farmhouse to the crops on unpaved road. The tractor left the farmhouse with the herbicide-tank full and came back with the tank empty;

(b) Application of the herbicide on the perimeter of the uncultivated field. Only the spray nozzles located on one side of the bar with respect to the H component were opened in such an operation;
(c) Application of the herbicide on the cultivated area. The tractor wheels remained between the planting rows and, when the machine reached the end of the row, it performed a U-curve crossing the planting rows;
(d) Braking: this occurred about five times each travel.

**Table 1.**

Strain measurements have been performed on the H component in some control points **[35]**. More precisely, two tee-rosettes have been arranged on each chord (see points W1 and W2 in **Figure 5**), whereas two fish-bone strain gauges have been arranged on one of the two braces (see point W3 in **Figure 5**).

For each of the manuevers listed in **Table 1**, the maximum principal strain time-history has been computed by exploiting such experimental measurements. Note that, for a given maneuver, an averaging operation (due to symmetry reasons) has been performed on the maximum principal strain time histories at point W1 and W2, and one time history has been obtained. The time histories are named $\varepsilon_{1,c}^{exp,m}$ at point W1 (or equivalently at point W2) and $\varepsilon_{1,b}^{exp,m}$ at point W3, being $1 \leq m \leq 12$ the index which corresponds to the maneuver number shown in **Table 1**.

In order to determine the multiaxial random stress field in the H component, finite element analyses have been carried out **[35]**. In more detail, the forces on the H component are schematised by $F_b$ and $F_c$ in **Figure 5**. The material is C25E steel, whose mechanical properties are listed in **Table 2**.

**Table 2.**

Linear elastic finite element analyses have been performed through the commercial package Ansys 14.5 (Work-bench 15.0) using SOLID 185 finite elements, both prismatic (8 nodes) and tetrahedral (10 nodes). The adopted discretization is shown in **Figure 7**, where the finite element mesh is assessed through a convergence analysis, being the minimum finite element size equal to about 0.7 mm. Details on the numerical model are available in Refs **[35,38]**.

**Figure 7.**

Initially, four forces $F_b$ have been applied to the FE model, each one being equal to 1N (in such a case, the $F_c$ force has been taken equal to zero). From the FE analysis, the maximum principal strain at point W1 is equal to about zero, whereas that at point W3 is 10 times greater. Then, one force $F_c$ equal to 1N has been applied to the FE model (in such a case, the $F_b$ forces have been taken equal to zero). From the FE analysis, the maximum principal strain at point W3 is equal to about zero, whereas that at point W1 is 110

times greater. Therefore, the maximum principal strain $\varepsilon_{1,c}^{num}$ at point W1 is only linked to the force $F_c$, whereas the maximum principal strain $\varepsilon_{1,b}^{num}$ at point W3 is only linked to the forces $F_b$.

Under linear elastic behaviour assumption, the numerical loading condition to simulate the actual one for the $m$-th maneuver, i.e. $F_b^m$ together with $F_c^m$ $(1 \le m \le 12)$, is obtained multiplying the unit value of $F_b^m$ or $F_c^m$ by the sequence $\varepsilon_{1,b}^{exp,m} / \varepsilon_{1,b}^{num}$ and $\varepsilon_{1,c}^{exp,m} / \varepsilon_{1,c}^{num}$, respectively. This operation ensures that $\varepsilon_{1,b}^{num,m} = \varepsilon_{1,b}^{exp,m}$ and $\varepsilon_{1,c}^{num,m} = \varepsilon_{1,c}^{exp,m}$ for each value of $m$, with $1 \le m \le 12$. Note that such an operation is possible since only static behaviour of the H component is considered, whereas dynamic behaviour (for example, due to resonance peaks or damping) is ignored.

### 3.2 Damage evaluation

Let us consider the polar frame $Or\alpha$ shown in **Figure 8**. The line starting from point $O$ with an orientation $\alpha$ can be considered as a generic extrapolation path according to the structural hot spot stress approach (described in Section 2.1). Therefore, the generic hot spot is the point at the intersection between such a line and the weld toe.

**Figure 8.**

The stress tensor at such a hot spot point is computed through Eqs (1)-(3) for each maneuver, where the thickness $T$ of the chord is equal to 4.76mm.

The damage is computed through Eq.(17) for each maneuver (the observation period $T_0$ in such an equation corresponds to the duration of each maneuver, see **Table 1**), and each value obtained is then multiplied by the number of times that a given maneuver is repeated during the observation time interval $\bar{T}$ (see last column of **Table 1**). The fatigue parameters used in such a calculation refer to welding material, and are listed in **Table 3**. The total damage is determined by summing the damage accumulated for each maneuver during $\bar{T}$.

**Table 3.**

Both stress tensor and damage calculation are repeated by varying $\alpha$, with $0° \le \alpha < 360°$.

The same procedure is performed for the brace by considering (a) the generic extrapolation path corresponding to a generator of the brace cylindrical surface, (b) the generic hot spot at the weld toe, (c) $T$ = 4.76mm, and by replacing $\sigma_x, \sigma_y, \tau_{xy}$ with $\sigma_z, \sigma_\theta, \tau_{z\theta}$ in Eqs (1)-(3).

## 4. RESULTS AND DISCUSSION

In **Figure 9**, the probability density function of the stresses $\sigma_{x,hs}, \sigma_{y,hs}, \tau_{xy,hs}$ (input data of the criterion) and the equivalent stress amplitude $\sigma_{eq,a}$ (output of the criterion) in the chord are shown for orientation $\alpha = 120°$ and maneuver $m = 4$ (**Figure 9(a)**) and $m = 6$ (**Figure 9(b)**). Such an orientation is that along which the accumulated total damage is maximum with respect to the other orientations, whereas the maneuvers $m = 4$ and $m = 6$ are those in correspondence of which the accumulated damage for $\alpha = 120°$ is maximum and minimum, respectively, in comparison with the other maneuvers being examined. A comparison between the shape of the input signals and that of the output signal can also be performed.

**Figure 9.**

The spectra of the maximum normal stress $N^*_{max}$, shear stress amplitude $C^*_a$, and equivalent stress amplitude $\sigma_{eq,a}$ in the chord are plotted in the case of $\alpha = 120°$, for maneuver $m = 4$ (**Figure 9(c)**) and $m = 6$ (**Figure 9(d)**). From such curves, the number of loading cycles for which the maximum value or amplitude of the above stresses is greater than a given value can be deduced.

**Figure 10** refers to the brace and is analogous to **Figure 9** but, in such a case, the orientation along which the accumulated damage is maximum is $\alpha = 105°$. For such an orientation, the maneuvers in correspondence of which the accumulated damage is maximum and minimum are the maneuvers $m = 4$ and $m = 3$, respectively.

**Figure 10.**

In **Figure 11**, the value of total damage is plotted against $\alpha$ in the chord (**Figure 11(a)**) and in the brace (**Figure 11(b)**). An $\alpha$ increment of 15° is selected.

**Figure 11.**

A critical damage $D_{cr} = 0.3$ is considered. As a matter of fact, it has been experimentally proved **[41,42]** that the critical damage is a random parameter that may range from 0.15 to 1.06. In more detail, the German guideline "Fracture Mechanics Proof of Strength of Engineering Components" **[41]** and Li et al. **[42]** recommended to adopt $D_{cr} = 0.3$ in design of steel structures, steel for casting, and aluminium alloy for mechanical components.

From **Figure 11**, it can be observed that the total damage is greater than the critical one for $38° \le \alpha \le 154°$ in the chord, whereas $48° \le \alpha \le 137°$ in the brace. **In Figure 3**, typical hot spots are shown. They have been observed for $\alpha$ equal to about $71°$ and $110°$, values extracted by a digitalisation procedure of failure zone pictures. Since such experimental values fall inside the above numerical $\alpha$-intervals, it can be concluded that the procedure proposed seems to identify, with significant accuracy, the region on the weld toe where cracks are expected to nucleate.

## 5. CONCLUSIONS

A novel procedure for fatigue resistance assessment of welded joints under complex random loading has been herein proposed. Through the extrapolation equation determined by means of the structural hot spot stress approach, damage at the verification point and consequently fatigue life are evaluated by applying the multiaxial critical plane-based criterion by Carpinteri et al. for random loading.

The novel procedure has been verified by examining a case study represented by the H component of an arm sprayer (used in agriculture) constituted from welded tubular elements fillet-welded as T-joints under the multiaxial random stress field. The procedure has been applied to evaluate the region on the weld toe where cracks are expected to nucleate, both in the chord and in the brace.

The comparison between experimental and numerical results in terms of crack nucleation location is quite satisfactory. The present approach seems to be a promising engineering tool able to identify the region on the weld toe where cracks are expected to nucleate and, consequently, to design a suitable reinforcement of such a region.

**Acknowledgements**

The authors gratefully acknowledge the financial support of the Italian Ministry of Education, University and Research (MIUR), Research Grant PRIN 2017 No. 2017HFPKZY on “Modelling of constitutive laws for traditional and innovative building materials”.

**REFERENCES**

**[1]** Thomas D.J. Analyzing the Failure of Welded Steel Components in Construction Systems, Journal of Failure Analysis and Prevention 2018; 18: 304–314.

**[2]** Paris P., Erdogan F., A Critical Analysis of Crack Propagation Laws, J. Basic Eng. 1963; 85: 528-533.

**[3]** Eurocode 3 - Design of steel structures - Part 1-1: General rules and rules for buildings, ENV 1993-1-1:2014.

**[4]** Unfired Pressure Vessels, EN 13445 Part 3: Design, European Committee for Standardization, 2014.

**[5]** Hobbacher A.F., Recommendations for Fatigue Design of Welded Joints and Components 2016, Second Edition, Springer.

**[6]** Lawrence F.V., Mattos R.J., Higashida Y., Burk J.D., Estimating the fatigue crack initiation life of welds. ASTM STP 1978: 648; 134–58.

**[7]** Radaj D., Review of fatigue strength assessment of non-welded and welded structures based on local parameters. International Journal of Fatigue 1996; 18: 153–70.

**[8]** Dong P. A structural stress definition and numerical implementation for fatigue analysis of welded joints. International Journal of Fatigue 2001; 23: 865-876.

**[9]** Maddox S.J., Razmjoo G.R., Interim fatigue design recommendations for fillet welded joints under complex loading, Fatigue and Fracture of Engineering Materials and Structures 2001; 24: 329-337.

**[10]** Radaj D., Sonsino C.M., Fricke W., Fatigue Assessment of Welded Joints by Local Approaches, Woodhead Publishing, 2006.

**[11]** Karakas O., Morgenstern C., Sonsino C.M., Fatigue design of welded joints from the wrought magnesium alloy AZ31 by the local stress concept with the fictitious notch radii of rf = 1.0 and 0.05 mm, International Journal of Fatigue 2008; 30; 2210-2219.

**[12]** Sonsino, C.M., Structural durability of welded constructions - Safety and reliability aspects in fatigue life assessment of

offshore tubular structures, Welding in the World 2008; 52: 123-130.
**[13]** Krzyzak D., Robak G., Łagoda T. Determining fatigue life of bent and tensioned elements with a notch, with use of fictitious radius, Fatigue and Fracture of Engineering Materials and Structures 2015; 38: 693-699.
**[14]** Meneghetti, G., De Marchi, A., Campagnolo, A., Assessment of root failures in tube-to-flange steel welded joints under torsional loading according to the Peak Stress Method, Theoretical and Applied Fracture Mechanics 2016; 83: 19-30.
**[15]** Yokozeki K., Miki C., Fatigue evaluation for longitudinal-to-transverse rib connection of orthotropic steel deck by using structural hot spot stress, Welding in the World 2016; 60: 83-92.
**[16]** Baumgartner J., Review and considerations on the fatigue assessment of welded joints using reference radii, International Journal of Fatigue 2017; 101: 459-468.
**[17]** Hemmesi K., Farajian M., Fatemi A. Application of the critical plane approach to the torsional fatigue assessment of welds considering the effect of residual stresses, International Journal of Fatigue 2017; 101: 271-281.
**[18]** Fricke W., Gao L., Paetzold H., Fatigue assessment of local stresses at fillet welds around plate corners, International Journal of Fatigue 2017; 101: 169-176.
**[19]** Karakaş Ö., Application of Neuber's effective stress method for the evaluation of the fatigue behaviour of magnesium welds, International Journal of Fatigue 2017; 101: 115-126.
**[20]** Łagoda T., Biłous P., Blacha Ł., Investigation on the effect of geometric and structural notch on the fatigue notch factor in steel welded joints, International Journal of Fatigue 2017; 101: 224-231
**[21]** Meneghetti G., Campagnolo A., Rigon D., Multiaxial fatigue strength assessment of welded joints using the Peak Stress Method – Part I: Approach and application to aluminium joints, International Journal of Fatigue, 2017; 101: 328-342.

**[22]** Meneghetti G., Campagnolo A., Rigon D., Multiaxial fatigue strength assessment of welded joints using the Peak Stress Method – Part II: Application to structural steel joints, International Journal of Fatigue 2017; 101: 343-362.
**[23]** Meneghetti G., Campagnolo A., Babini V., Sabbadin P., Multiaxial fatigue assessment of a structural steel joint according to the peak stress method, 2017. In proceedings of: ICF 2017 - 14th International Conference on Fracture 1, pp. 896-897.
**[24]** Karakaş Ö., Zhang G., Sonsino C.M., Critical distance approach for the fatigue strength assessment of magnesium welded joints in contrast to Neuber's effective stress method, International Journal of Fatigue 2018; 112: 21-35.
**[25]** da Silva A.L.L., Correia J.A.F.O., de Jesus A.M.P., , Calçada R., Lesiuk G., Fernandes A. A., Berto F. Influence of fillet end geometry on fatigue behaviour of welded joints, International Journal of Fatigue 2019; 123: 196-212.
**[26]** Grong Ø., Sandnes L., Berto F., Progress in solid state joining of metals and alloys, Procedia Structural Integrity 2019; 17: 788-798.
**[27]** Huang Y., Zhang Q., Bao Y, Bu Y., Fatigue assessment of longitudinal rib-to-crossbeam welded joints in orthotropic steel bridge decks, Journal of Constructional Steel Research 2019; 159: 53-66.
**[28]** Li J., Zhang Q., Bao Y., Zhu J., Chen L., Bu Y., An equivalent structural stress-based fatigue evaluation framework for ribto-deck welded joints in orthotropic steel deck, Engineering Structures 2019; 196: 109304.
**[29]** Luo P., Zhang Q., Bao Y. Predicting weld root notch stress intensity factors for rib-to-deck welded joint under deck loading modes, International Journal of Fatigue 2019; 128: in press.
**[30]** Rozumek D., Lewandowski J., Lesiuk G., Correia J.A., The influence of heat treatment on the behavior of fatigue crack growth in welded joints made of S355 under bending loading, International Journal of Fatigue 2020; 131, in press.

**[31]** Carpinteri A., Spagnoli A., Vantadori S., A multiaxial fatigue criterion for random loading. Fatigue and Fracture of Engineering Materials and Structures 2003; 26, 515-522.
**[32]** Carpinteri A., Fortese G., Ronchei C., Scorza D., Spagnoli A., Vantadori S., Fatigue life evaluation of metallic structures under multiaxial random loading, International Journal of Fatigue 2016; 90: 191–199.
**[33]** Carpinteri A., Spagnoli A., Vantadori S., A review of multiaxial fatigue criteria for random variable amplitude loads, Fatigue and Fracture of Engineering Materials and Structures 2017; 40: 1007–1036.
**[34]** Vantadori S., Iturrioz I., Ronchei C., Discussion on fatigue life estimation under multiaxial random loading: comparison between time- and frequency-domain approach, Theoretical and Applied Fracture Mechanics 2018; 96: 134-145.
**[35]** Giordani F A. Estudo de Metodologias para medir a vida em fadiga Multiaxial não proporcional, Master Thesis, Promec/UFRGS, Brazil,2015 [in Portuguese]. http://hdl.handle.net/10183/118864.
**[36]** Carpinteri A., Boaretto J., Fortese G., Giordani F., Iturrioz I., Ronchei C., Scorza D., Vantadori S., Fatigue life estimation of fillet-welded tubular T-joints subjected to multiaxial loading, International Journal of Fatigue 2017; 101: 263–270.
**[37]** Vantadori S., Boaretto J., Fortese G., Giordani F., Isoppo Rodrigues R., Iturrioz I., Ronchei C., Scorza D., Zanichelli A., Fatigue strength of welded joints under multiaxial non-proportional loading, Procedia Structural Integrity 2017; 5: 761-768.
**[38]** Carpinteri A., Boaretto J., Fortese G., Giordani F., Isoppo Rodrigues R., Iturrioz I., Ronchei C., Scorza D., Vantadori S., Zanichelli A., Welded joints under multiaxial non-proportional loading, Theoretical and Applied Fracture Mechanics 2018; 93: 202-210.
**[39]** Vantadori S., Giordani F., Fortese G., Iturrioz I., Hot-spot localisation according to the critical plane-based approach, International Journal of Fatigue 2018; 116: 669-676.

**[40]** Papadopoulos I.V., Critical plane approaches in high-cycle fatigue: on the definition of the amplitude and mean value of the shear stress acting on the critical plane, Fatigue Fract. Eng. Mater. Struct. 1998; 21: 269–285.

**[41]** FKM-Guideline, Analytical Strength Assessment of Components in Mechanical Engineering (5 ed.), German Council for Engineering Research, Forschungskuratorium Maschinenbau (FKM), Frankurt, Germany, 2003.

**[42]** Lee Y.L., Barkey M.E., Kang H.T., Metal Fatigue Analysis Handbook: Practical Problem – Solving Techniques for Computer-Aided Engineering (1 ed.), Butterworth- Heinemann, Massachusetts, USA, 2011.

**Submitted to International Journal of Fatigue**

VSI: Fatigue of Welded Joints – Current State-of-the-Art

January 2020

**Version R1, March 2020**

# A NOVEL PROCEDURE FOR DAMAGE EVALUATION OF FILLET-WELDED JOINTS

Sabrina Vantadori[1], Ignacio Iturrioz[2], Andrea Carpinteri[1], Fabrizio Greco[3], Camilla Ronchei[3]

[1]Department of Engineering & Architecture, University of Parma, Parco Area delle Scienze 181/A, 43124 Parma, Italy

[2]Mechanical Post- Graduate Program, Federal University of Rio Grande do Sul, Sarmento Leite 425, CEP 90050-170, Porto Alegre, Brazil

[3]Department of Civil Engineering, University of Calabria, via Pietro Bucci, 87036 Arcavacata di Rende (CS), Italy

## FIGURES AND TABLES

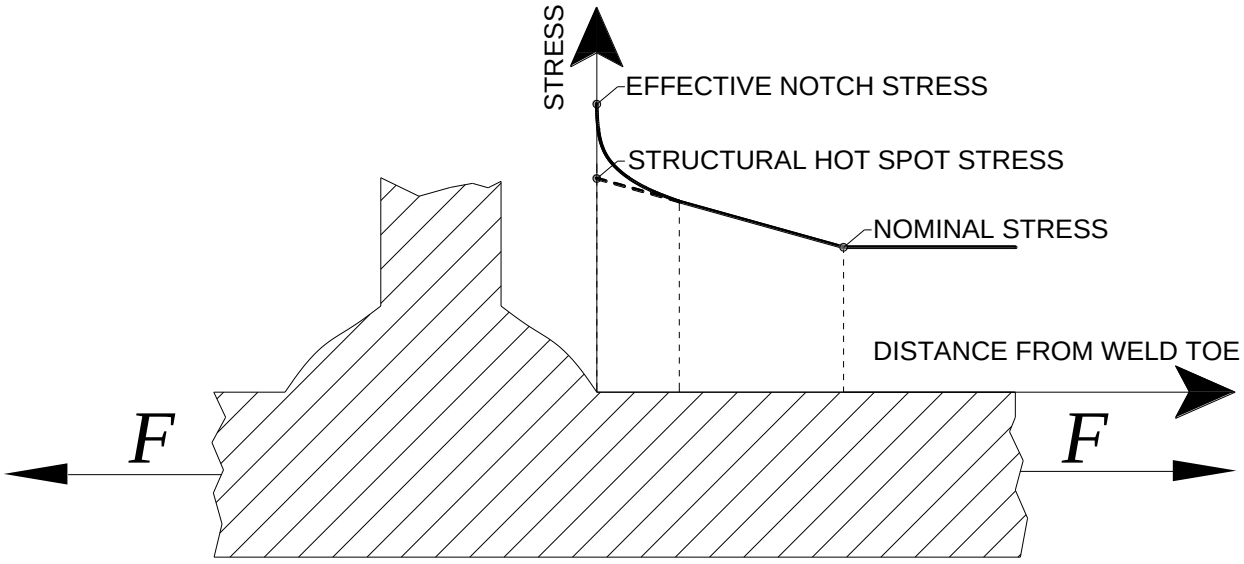


**Figure 1.** Three weld stress calculation methods.

Figure 2. H component of an arm sprayer used in agriculture.

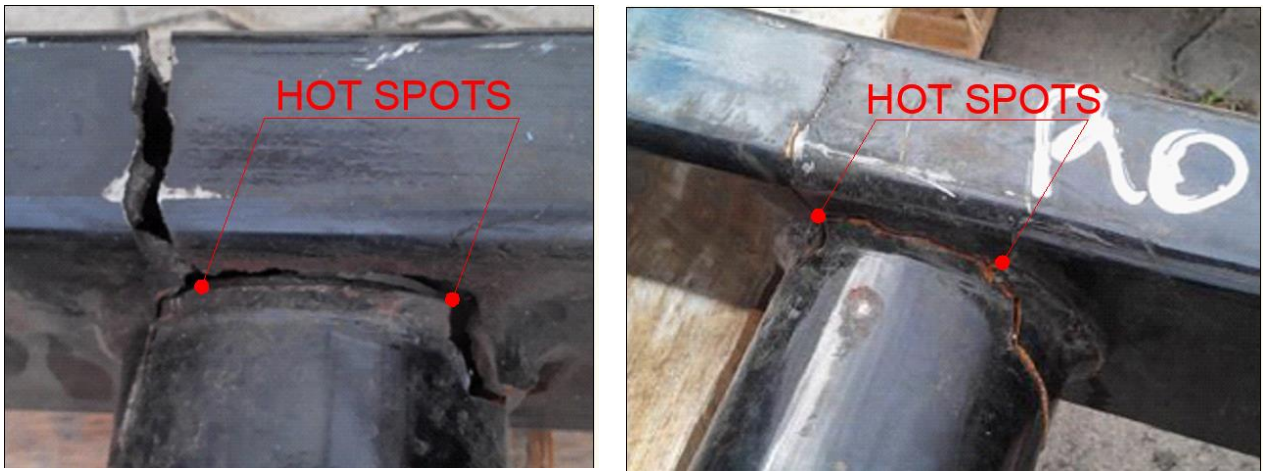


**Figure 3.** Typical examples of fatigue failure in the H component. The experimental hot spots are highlighted.

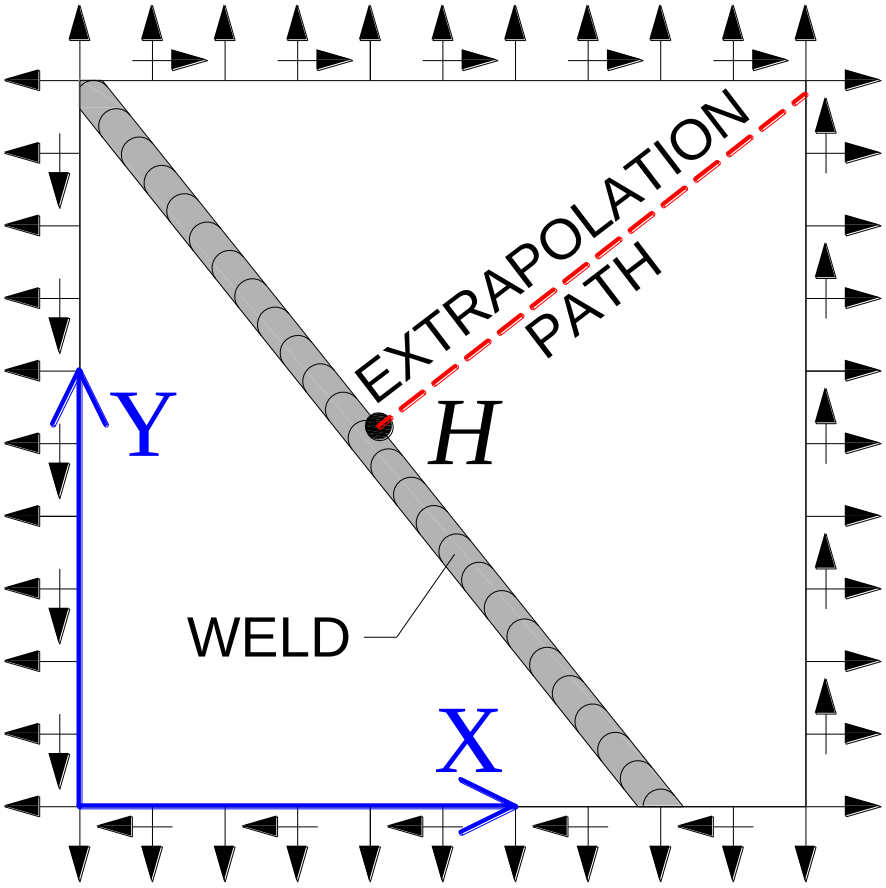


**Figure 4.** Hot spot and the corresponding extrapolation path according to the structural hot spot stress approach.

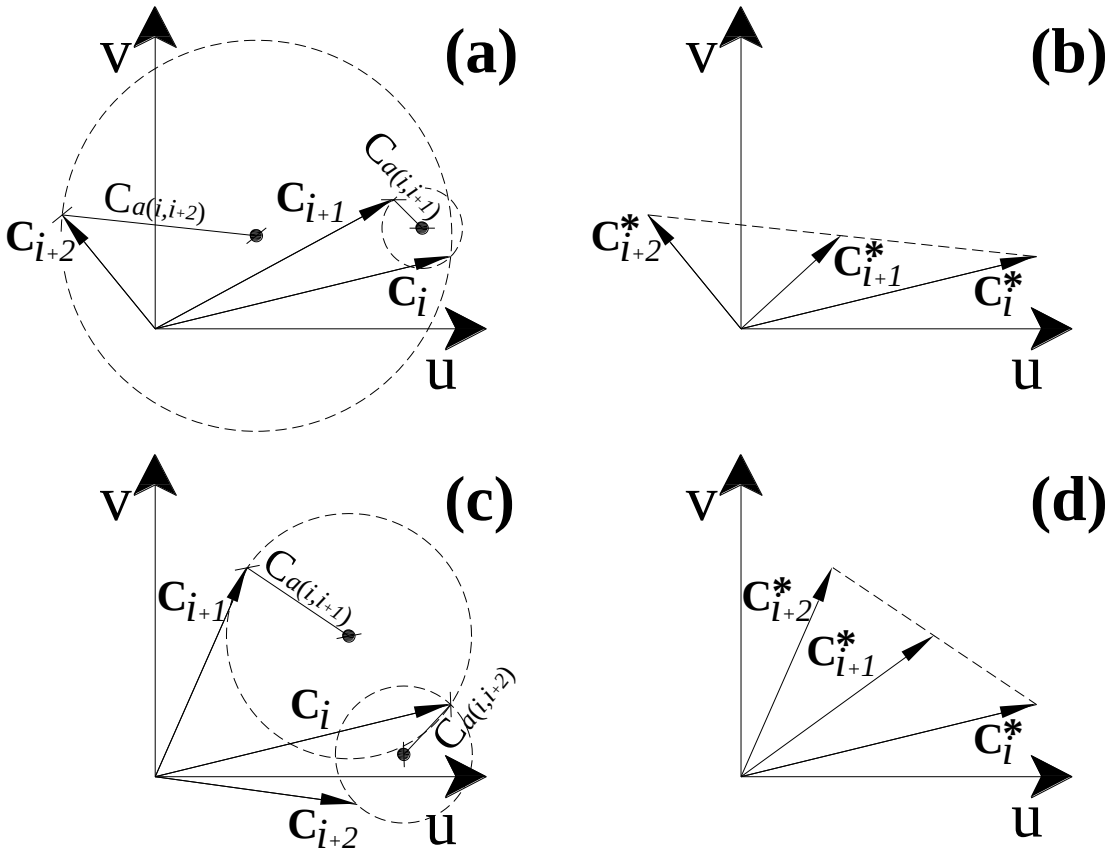


**Figure 5.** Reduction procedure on $\mathbf{C}$-series: (a) original series and (b) reduced series for $C_{a(i,i+1)} \le C_{a(i,i+2)}$; (c) original series and (d) reduced series for $C_{a(i,i+1)} > C_{a(i,i+2)}$.

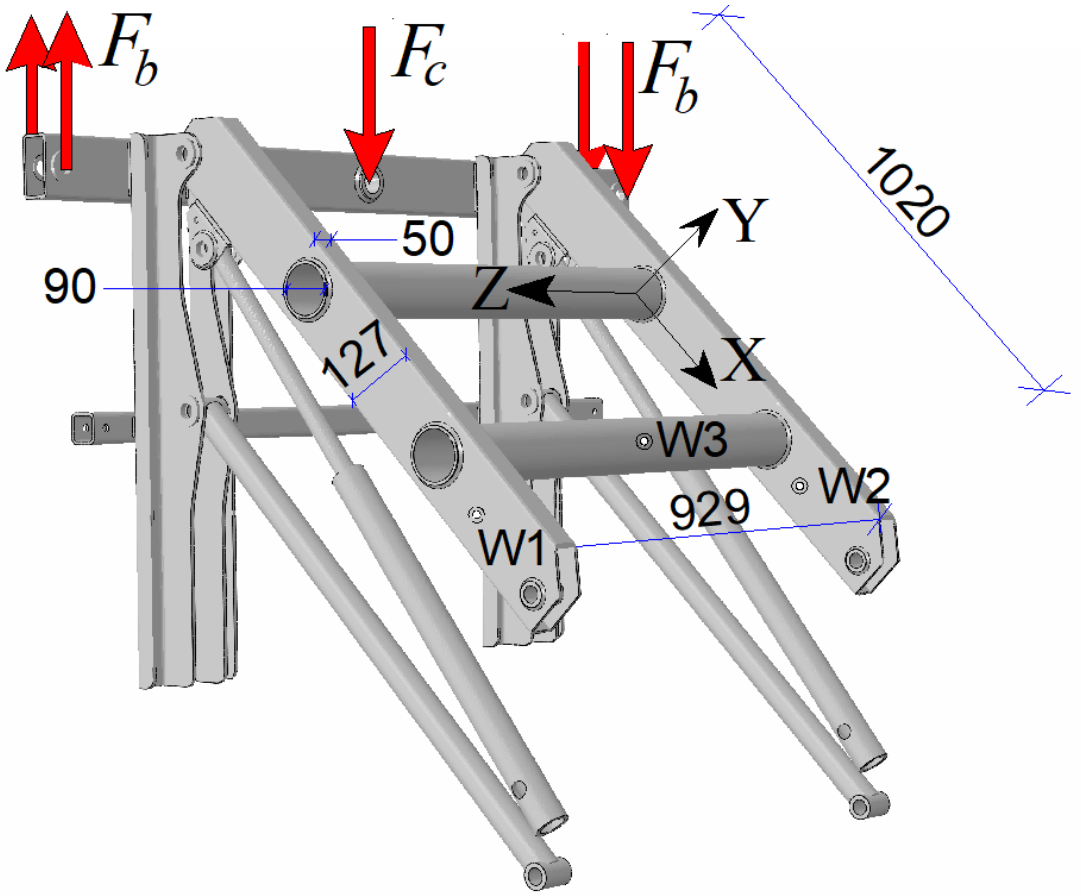


**Figure 6.** H component: geometrical sizes (in mm), loading condition and control points.

**Table 1.** Sprayer service condition: duration and number of repetitions of each maneuver during the observation time interval $\bar{T}$.

| MANEUVERS | No. | FUEL TANK | DURATION [s] | TIMES |
|---|---|---|---|---|
| Application of the herbicide (cultivated area) | 1 | Full | 180 | 9000 |
| | 2 | Empty | 140 | 11572 |
| Application of the herbicide (perimeter) | 3 | Full | 40 | 18000 |
| | 4 | Empty | 52 | 13847 |
| Braking | 5 | Full | 10 | 18293 |
| | 6 | Empty | 93 | 7827 |
| U - curves | 7 | Full | 150 | 2400 |
| | 8 | Empty | 39 | 9231 |
| Travel on unpaved road | 9 | Full | 115 | 3120 |
| | 10 | Empty | 46 | 7913 |
| Perimeter curves | 11 | Full | 19 | 18948 |
| | 12 | Empty | 37 | 9864 |

**Table 2.** Mechanical properties for C25E steel **[35].**

| MATERIAL | $E$ [GPa] | $\nu$ [-] | $\sigma_u$ [MPa] | $f_y$ [MPa] |
|---|---|---|---|---|
| C25E | 198.0 | 0.3 | 470.0 | $\geq$230.0 |

**Figure 7.** Discretization adopted for the finite element analysis **[38].**

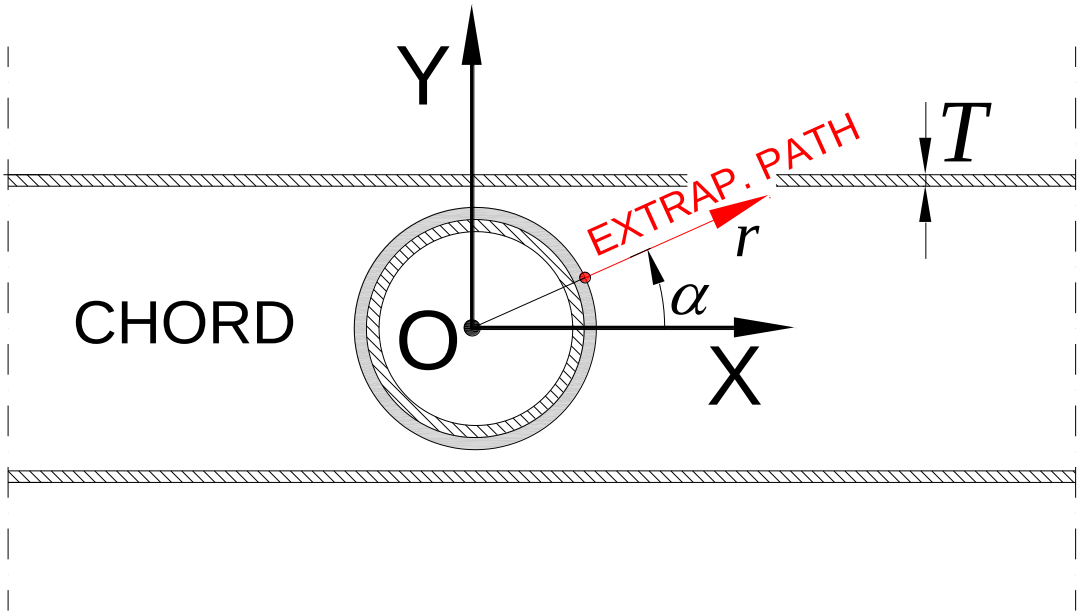


**Figure 8.** Polar frame $Or\alpha$ and extrapolation path for the chord.

**Table 3.** Fatigue properties for the welding [35].

| MATERIAL | $\sigma_{af,-1}$ [MPa] | $k$ | $\tau_{af,-1}$ [MPa] | $k^*$ | $N_0$ [cycles] | $N_0^*$ [cycles] |
|---|---|---|---|---|---|---|
| Welding | 25.0 | 3 | 18.0 | 5 | $5\,(10)^6$ | $10^8$ |

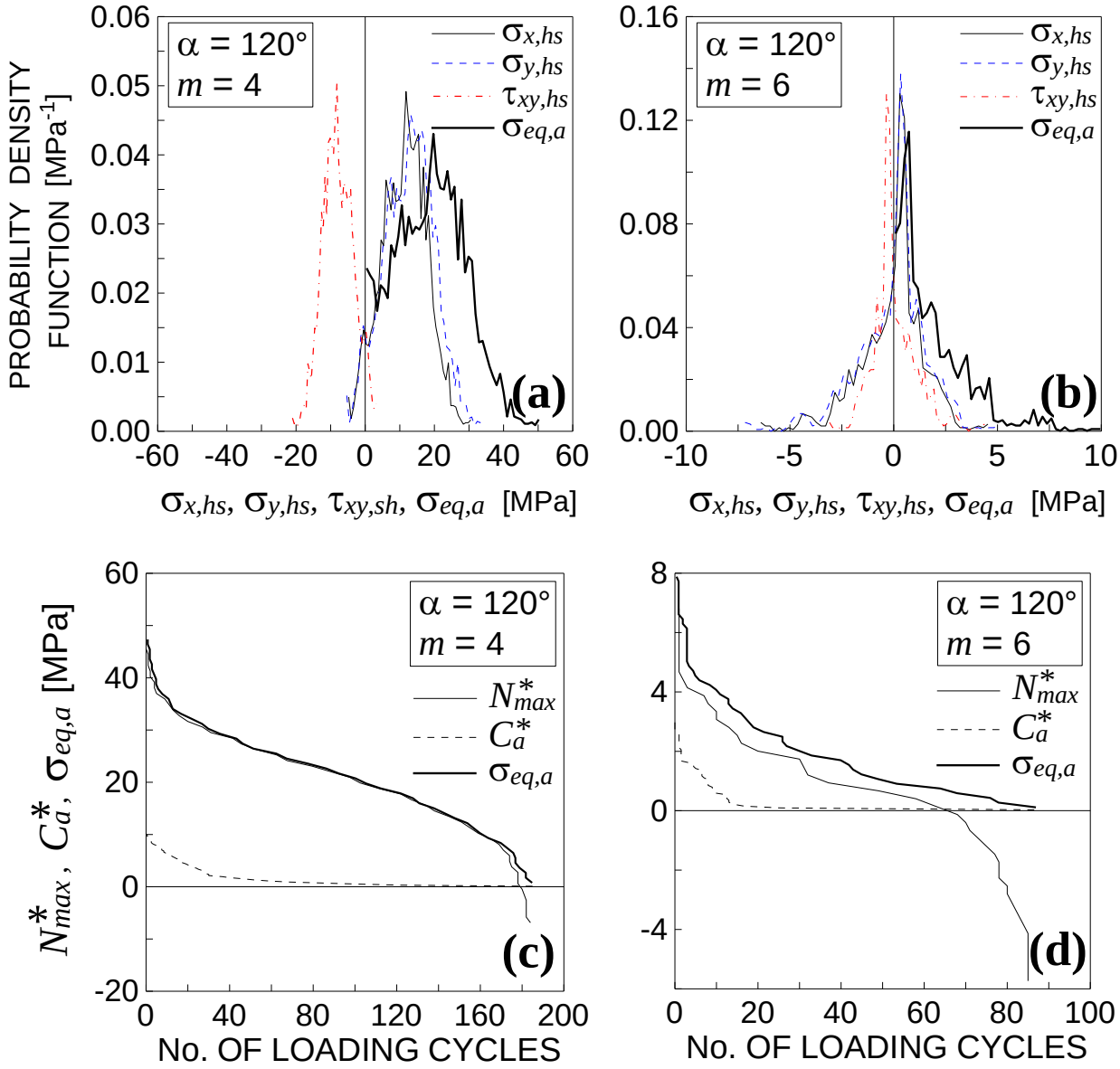


**Figure 9.** Probability density function of the hot spot stresses and the equivalent stress amplitude in the chord, for $\alpha = 120°$: (a) $m = 4$; (b) $m = 6$. Spectra of the maximum normal stress, shear stress amplitude and the equivalent stress amplitude in the chord, for $\alpha = 120°$: (c) $m = 4$; (d) $m = 6$.

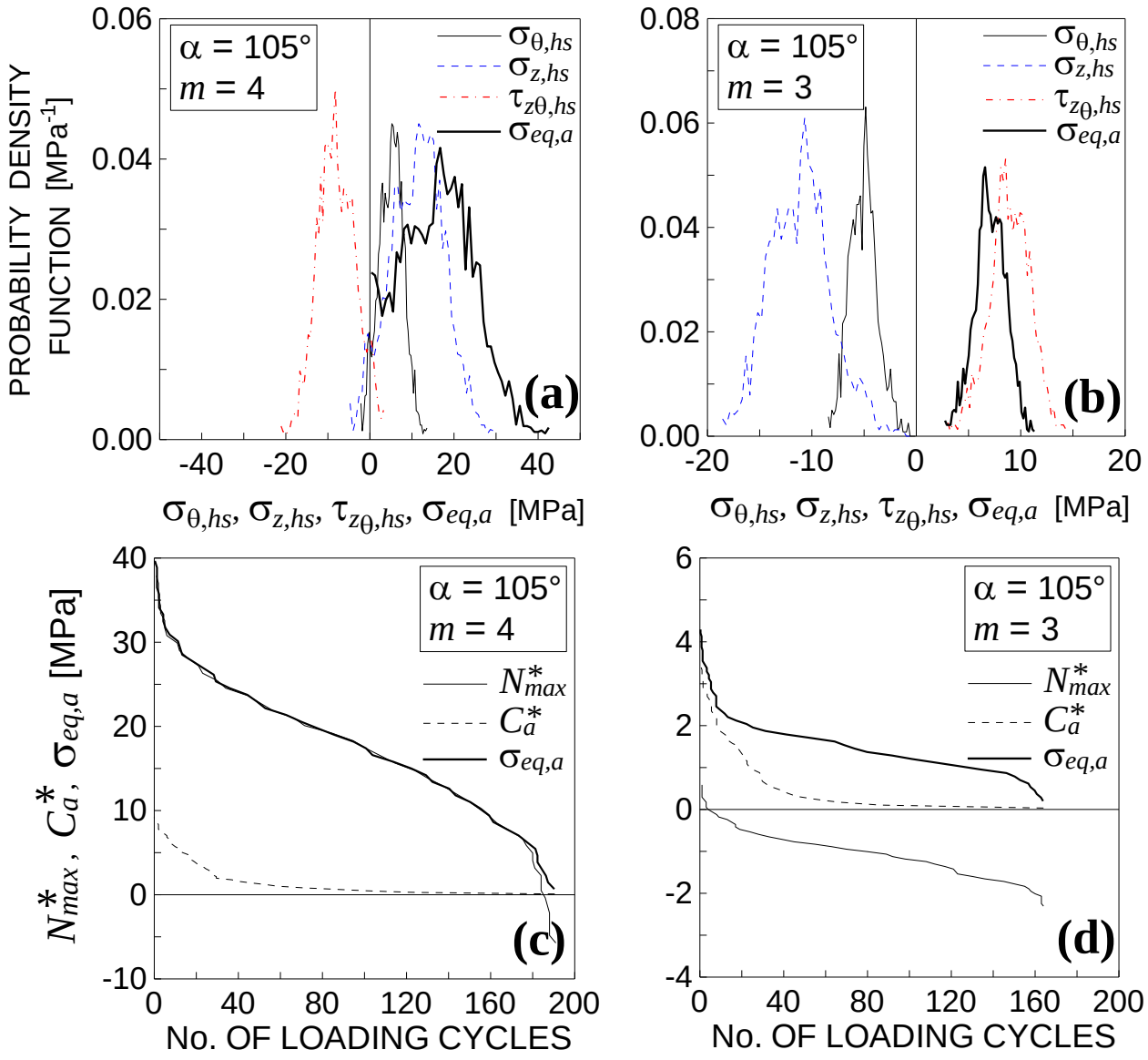


**Figure 10.** Probability density function of the hot spot stresses and the equivalent stress amplitude in the chord, for $\alpha = 105°$: (a) $m = 4$; (b) $m = 3$. Spectra of the maximum normal stress, shear stress amplitude and the equivalent stress amplitude in the chord, for $\alpha = 105°$: (c) $m = 4$; (d) $m = 3$.

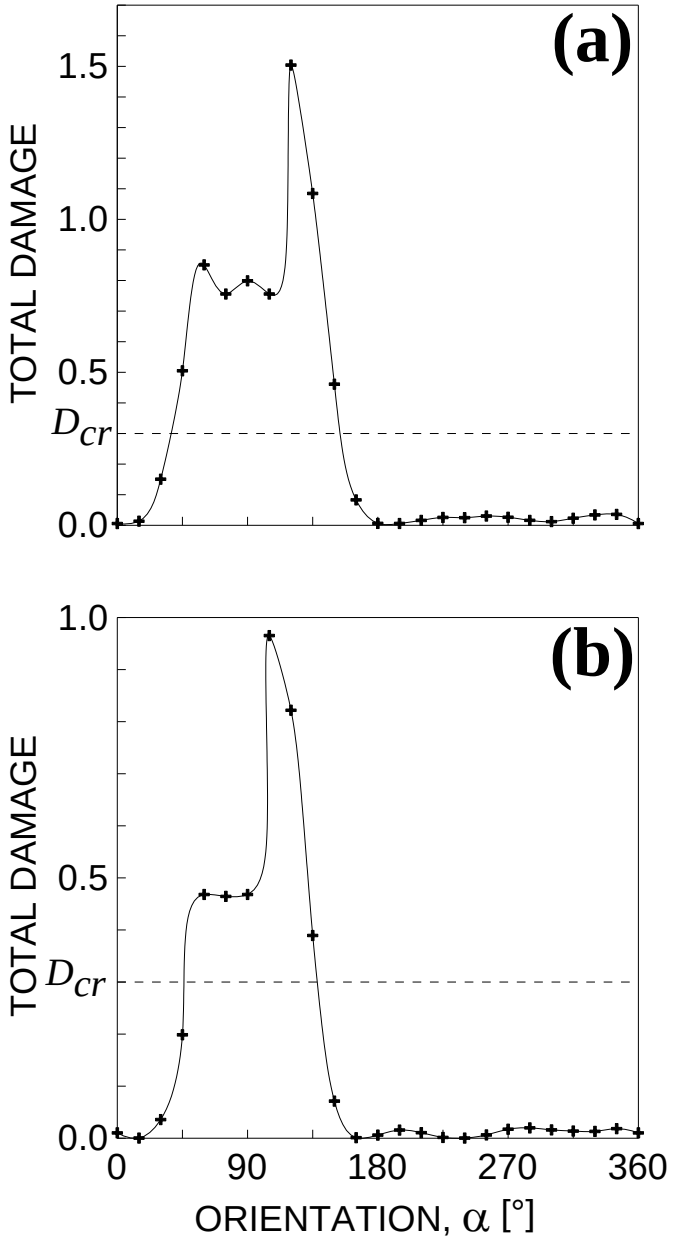


**Figure 11.** Total damage vs orientation $\alpha$: (a) chord; (b) brace.